# DESIGN, FABRICATION AND CHARACTERIZATION OF NOVEL HETEROJUNCTION AND HOMOJUNCTION ORGANIC SOLAR CELLS

*-Doctoral Thesis Summary-*


By

**Ing. Gavril-Ionel GIURGI**



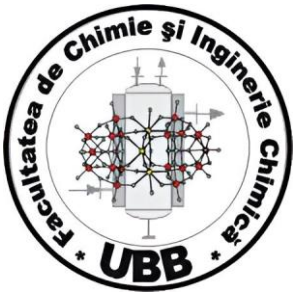




BABES-BOLYAI UNIVERSITY (UBB) OF CLUJ-NAPOCA
Faculty of Chemistry and Chemical Engineering

&

TECHNICAL UNIVERSITY OF CLUJ-NAPOCA (UTCN)
Faculty of Electronics, Telecommunications and Information Technology

Scientific Advisors: **Prof. Dr. Ion GROSU**
**Prof. Dr. Ing. Ramona -Voichița GĂLĂTUȘ**



CLUJ-NAPOCA, 2025

# Table of Contents

# Abbreviations and Acronyms

- **Al** – Aluminium
- **AFM** – Atomic Force Microscopy
- **BHJ** – Bulk Heterojunction
- **Bphen** – Bathophenanthroline
- **$C_{60}$/$C_{70}$** – Fullerene
- **CB** – Chlorobenzene
- **CF** – Chloroform
- **DCB** – Dichlorobenzene
- **DCV** – Dicyanovinyl
- **EQE** – External Quantum Efficiency
- **ETL** – Electron Transport Layer
- **FF** – Fill Factor
- **HOMO** – Highest Occupied Molecular Orbital
- **HOSCs** – Homojunction Organic Solar Cells
- **HTL** – Hole Transport Layer
- **IDT** – Indacenodithiophene
- **ITO** – Indium Tin Oxide
- **$J_{SC}$** – Short-Circuit Current Density
- **LUMO** – Lowest Unoccupied Molecular Orbital
- **NFAs** – Non-Fullerene Acceptors
- **$MoO_3$** – Molybdenum Trioxide
- **OSCs** – Organic Solar Cells
- **$PC_{61}BM$** – (Phenyl-$C_{61}$-butyric acid methyl ester)
- **P3HT** – Poly(3-hexylthiophene)
- **PCE** – Power Conversion Efficiency
- **PEDOT:PSS** – Poly(3,4-ethylenedioxythiophene) polystyrene sulfonate
- **PET** – Polyethylene Terephthalate
- **PHJ** – Planar Heterojunction
- **PTB7** – Poly(thiophene-benzodithiophene)
- **SMOSCs** – Single Material Organic Solar Cells
- **$V_{OC}$** – Open-Circuit Voltage
- **ZnO** – Zinc Oxide

# General Introduction

The increasing global demand for electricity, driven by industrial growth and new technologies, is accelerating fossil fuel depletion and $CO_2$ emissions, reinforcing the need for renewable energy sources.[1] Among them, organic solar cells (OSCs) stand out in third-generation photovoltaics, offering a lightweight, flexible, and cost-effective alternative to silicon-based technology. Despite efficiency improvements (e.g., 20.82% for OSCs), their relatively short lifespan remains a challenge, making research on stability and scalability essential.[2, 3]

**Main Objective**

This thesis focuses on the development and optimization of new single-material organic solar cells (SMOSCs) based on both heterojunction and homojunction types. The research explores novel approaches for creating efficient organic photovoltaic devices in which a single material serves as both the donor and the acceptor, providing a simplified and scalable alternative to traditional OSC structures.

**Thesis Structure**

- **Chapter 1**: Reviews the fundamental principles of OSCs, including their types, structures, and materials.
- **Chapter 2**: Focuses on optimizing bulk heterojunction (BHJ) and planar heterojunction (PHJ) OSCs using both commercial donor/acceptor materials and newly synthesized molecules from our laboratory.
- **Chapter 3**: Presents experimental results for OSCs on glass substrates, focusing on heterojunction and homojunction SMOSCs and analyzing the impact of different molecular structures on their performance. Additionally, it includes studies on BHJ and PHJ structures using newly synthesized small donor molecules and non-fullerene acceptors (NFAs).
- **Chapter 4**: Investigates OSCs on flexible PET substrates, comparing their performance to those on glass. It also explores the integration of flexible OSCs in series or parallel configurations using 3D-printed masks to enhance electrical output, concluding with tests on flexible OSC arrays for powering low-energy devices.

# Chapter 1: Literature Data

## 1.1 Introduction

The research on solar energy and photovoltaic technologies, including organic solar cells (OSCs), has gained significant attention due to their potential to contribute to global electricity generation.[1] The photovoltaic effect, first observed by Alexandre E. Becquerel in 1839, is the fundamental principle behind solar cell operation.[4] Since the development of the first silicon solar cell in 1953 at Bell Laboratories, photovoltaic (PV) technology has evolved, leading to efficiency improvements and cost reductions.[5]

Organic semiconductors, composed of carbon-based compounds, were first studied in the early 20th century, with notable advancements made by Ching Tang in 1986 when he developed the first bilayer donor-acceptor (D/A) junction OSC with 1% efficiency.[6] The introduction of bulk heterojunction (BHJ) solar cells further enhanced efficiency, leading to the rapid development of organic PV technology. Today, single-junction BHJ OSCs can achieve efficiencies of 19.2% to 20.8%, driven by advancements in organic semiconductor research and material processing techniques.[2]

## 1.2 Working Principle and Characterization of OSCs

OSCs consist of donor and acceptor materials that form a thin film structure between two electrodes. Unlike inorganic solar cells, organic semiconductors have a low dielectric constant, requiring the formation of excitons (electron-hole pairs) upon light absorption. The operational process of OSCs includes five key steps: 1) Absorption of light and generation of excitons; 2) Diffusion of excitons to the donor-acceptor (D/A) interface; 3) Dissociation of excitons into charges due to energy differences, with electron transfer from the donor's LUMO to the acceptor's LUMO; 4) Migration of charges to the corresponding electrodes; 5) Collection of electrons at the cathode and holes at the anode, generating photocurrent.[8]

To evaluate the performance of OSCs, key parameters such as open-circuit voltage ($V_{OC}$), short-circuit current density ($J_{SC}$), fill factor (FF), and power conversion efficiency (PCE) are determined through current-voltage (J-V) measurements. The external quantum efficiency (EQE) spectrum is also analyzed to assess the absorption efficiency of the solar cell.[9]

## 1.3 Types of OSCs

There are several OSC architectures, each with its strengths and limitations:

**1.3.1 Single-layer** : Simple Schottky diode-like devices with limited efficiency due to poor charge separation.[10]

**1.3.2 Planar bilayer heterojunction**: Introduced by Ching Tang in 1986, these improve charge separation but are limited by short exciton diffusion lengths (~10-20 nm).[6]

**1.3.3 Bulk heterojunction (BHJ)**: A significant improvement over bilayer structures, BHJ OSCs enhance charge separation and light absorption by forming an interpenetrating donor-acceptor network. To optimize OSC performance, various methods are employed, such as solvent additives, thermal and solvent vapor annealing, and controlled phase segregation.[11]

**1.3.4 Advancements in OSC Architectures**

*Conventional vs. Inverted OSCs*: Conventional OSCs use ITO as the anode, with PEDOT:PSS as the hole transport layer (HTL). However, due to stability issues, inverted OSCs were developed, where ITO functions as the cathode with ZnO as electron transport layer (ETL), improving device stability and efficiency.[11, 12]

*Tandem OSCs*: Multi-junction devices stack multiple active layers to optimize light absorption across the solar spectrum, leading to higher efficiency.[13]

## 1.4 Organic Materials for OSCs

The efficiency of OSCs depends largely on the donor and acceptor materials used in the active layer.

**1.4.1 Donors:**

*Polymer donors*: Among the most well-known is P3HT, which has been extensively studied but exhibits limited light absorption.[14] Donor-type polymers with a more complex structure, such as PTB7 [Poly(thienothiophene-benzodithiophene)7] and PBTT [Poly(benzodithiophene-thiophene-thiophene)], have achieved performances of up to 10%. The most advanced generations of copolymers, such as D16 (Benzodithiophene with furans, BDT-F) and D18 (Naphthalene-dithiophene with furans, NDT-F), have demonstrated efficiencies exceeding 16-18% when combined with non-fullerene acceptors (NFAs).[15, 16]

*Small molecule donors*: These materials, including oligothiophenes, merocyanine derivatives, and BDT-based compounds (BTR, BTR-Cl) – the latter achieving performances of 10-15% – offer better synthesis control and high reproducibility.[17]

**1.4.2 Acceptors:**

*Fullerene Acceptors*: Derivatives like $C_{60}$, $C_{70}$, $PC_{61}BM$ and $PC_{71}BM$ have been widely used due to their high electron mobility. However, they suffer from limited tunability and absorption in the visible spectrum.[18, 19]

*Non-Fullerene Acceptors (NFAs)*: New classes of acceptors, including perylene diimide (PDI) derivatives, indacenoditriazole derivatives, and those based on indacenodithiophenothiophene, have demonstrated superior absorption and efficiency compared to fullerene acceptors. The use of non-

fullerene acceptors has enabled OSCs to achieve efficiencies of 18-20%.[7, 20]

### 1.5 Chapter's conclusions

This chapter provides an overview of the history, working principles, and advancements in OSC technology. By analyzing different device architectures and organic semiconductor materials, it highlights the potential of OSCs in renewable energy applications. The progress in efficiency and stability paves the way for further research into optimizing organic photovoltaic materials and manufacturing processes.

# Chapter 2: Optimization of bulk & planar heterojunction OSCs

This chapter systematically analyzes the key factors influencing the performance of bulk heterojunction (BHJ) and planar heterojunction (PHJ) organic solar cells (OSCs), focusing on structural and processing optimizations.

## 2.1 Improvement of classic BHJ OSCs parameters

For BHJ OSCs, a comparative study between conventional and inverted structures (Figure 2.1) using P3HT:$PC_{61}BM$ (1:1) demonstrated that thermal treatment significantly improves photovoltaic performance. The inverted structure achieved a superior efficiency of 3.05% at 180°C, compared to 2.29% at 160°C for the conventional structure.

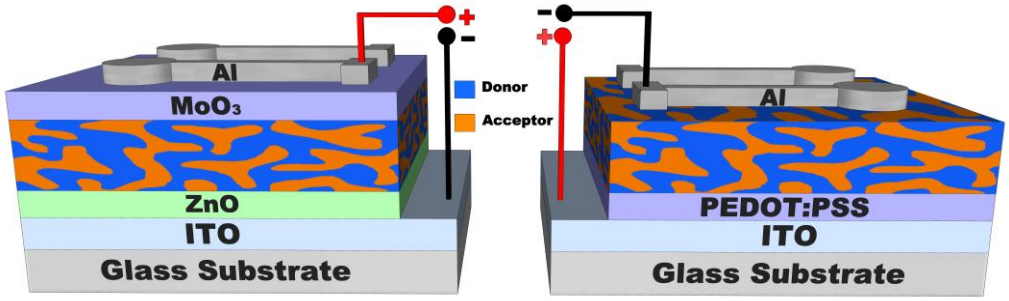


**Figure 2.1.** Inverted bulk structure (left) vs. direct (right)

Similarly, thermal treatment enhanced the efficiency of P3HT:1 (1-a small molecule acceptor from **Figure 2.2)** in the inverted BHJ structure from 0.6% (as-cast) to 1.72% at 120°C.

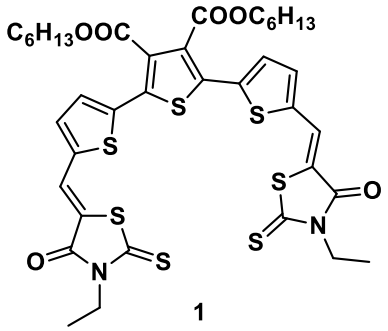


**Figure 2.2.** Chemical structure of the NFA acceptor **1**

The effect of solvents and additives was also investigated for the PTB7:$PC_{61}BM$ (1:1.5, w:w) system in the inverted BHJ structure.The best solvent was chlorobenzene (CB) (PCE = 3.89%), followed by CF:CB (1:1) (PCE = 3.52%) and dichlorobenzene (DCB) (PCE = 3.39%). Adding 1,8-diiodooctane (DIO, 3%) and diphenyl ether (DPE, 3%) further increased efficiency to 5.16% and 4.76%, respectively.

## 2.2 Optimization of the parameters for BHJ OSCs with small molecule donors and $PC_{61}BM$ acceptor

For small-molecule donors (2 and 3 from **Figure 2.3**) paired with $PC_{61}BM$, the inverted BHJ architecture outperformed the conventional structure, achieving 2.00% (2:$PC_{61}BM$) and 1.30% (3:$PC_{61}BM$) compared to 1.54% and 0.86%, respectively.[21, 22]

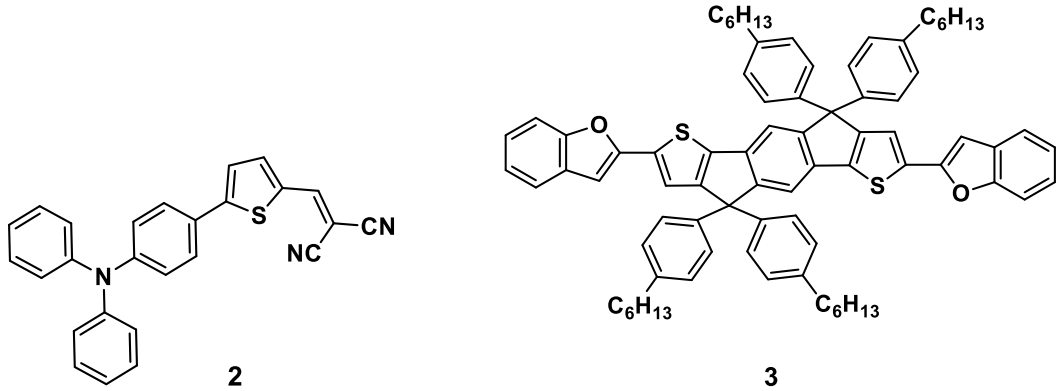


**Figure 2.3.** Chemical structure of donors **2** and **3**

Optimizing the donor-acceptor ratio (1:2 w/w) and buffer layer thicknesses (ZnO: 30 nm, $MoO_3$: 10 nm) played a crucial role in performance enhancement. Stability tests confirmed the superior longevity of the inverted BHJ structure (1.07% efficiency after 50 days) compared to the direct structure (0.08% after 10 days).[21]

## 2.3. Improvement of parameters for PHJ-type OSCs

For PHJ OSCs, the inverted architecture (ITO/ZnO/$C_{60}$/4 or 5/$MoO_3$/Al) achieved a ~45% increase in efficiency compared to the direct structure (ITO/PEDOT:PSS/4 or 5/$C_{60}$/Al). Efficiency improved from 0.64% to 1.12% for donor 4 and from 0.87% to 1.56% for donor 5. The optimal thicknesses for donor (20 nm), acceptor (30 nm), and $MoO_3$ (HTL, 16 nm) were identified.[23]

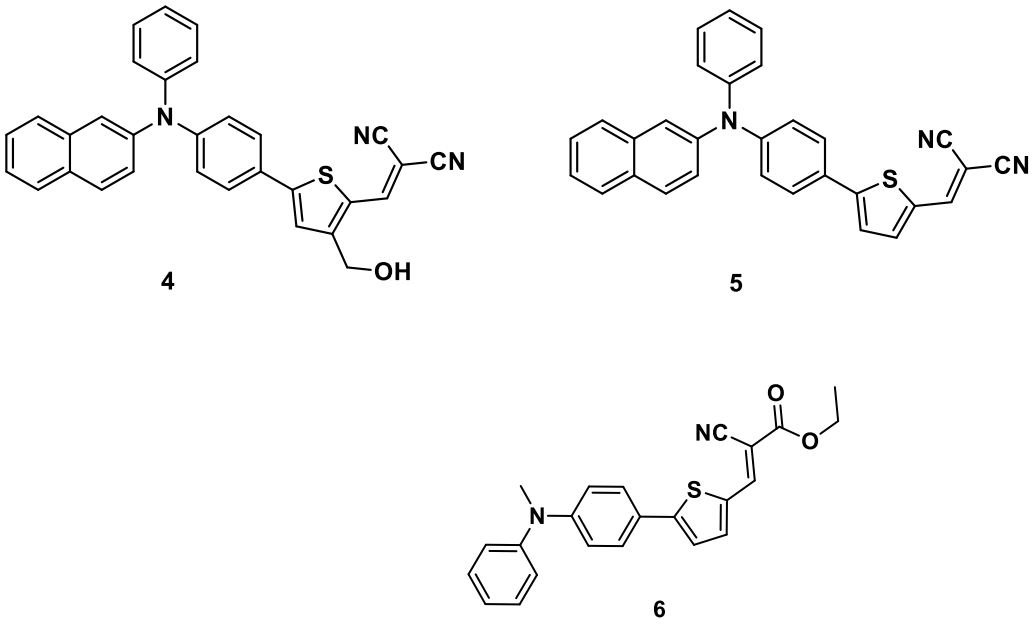


**Figure 2.4** Chemical structures for the donors **4** ,**5** and **6**

Lastly, the inclusion of $MoO_3$ and Bphen buffer layers in direct PHJ OSCs significantly improved efficiency, closing the gap with the inverted structure (Figure 2.5).[24]

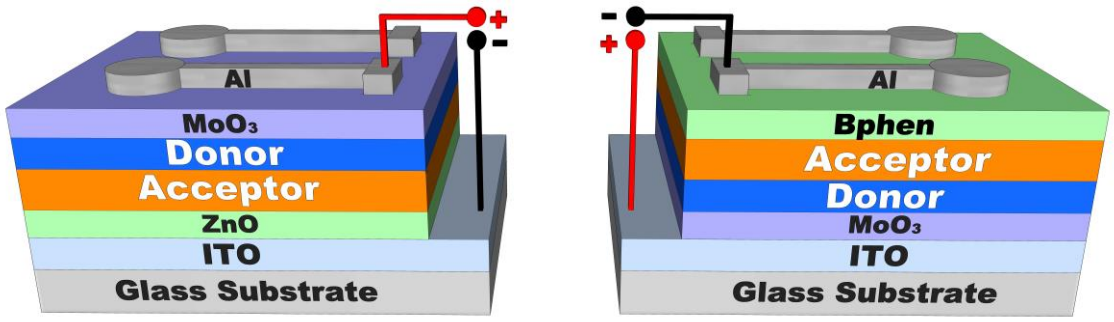


**Figure 2.5 .** Representations of the inverted-PHJ (left) and direct-PHJ OSC architectures with $MoO_3$ and Bphen buffer layers (right)

The direct PHJ structure (ITO/$MoO_3$/6/$C_{70}$/Bphen/Al) achieved 1.25% efficiency, approaching that of the inverted PHJ (1.37%). $MoO_3$ improved hole mobility and stability, while Bphen enhanced electron transport and protected the active layer.[24]

## 2.4 Chapter's Conclusions

This chapter systematically analyzed key factors influencing BHJ and PHJ OSC performance using commercial and newly synthesized organic molecules.

- Inverted BHJ structures consistently outperformed conventional ones, demonstrating higher efficiency and stability. Thermal treatment significantly improved photovoltaic performance, while solvent and additive selection further enhanced efficiency.
- Inverted PHJ architectures also showed superior efficiency, with $MoO_3$ and Bphen buffer layers

reducing the gap between direct and inverted configurations. These findings provide a strong basis for further optimization and the development of high-performance OSCs.

These optimizations establish a solid foundation for developing high-performance OSCs using novel organic small molecules, which are further analyzed in the following chapters.

# Chapter 3: Investigation of Novel Organic Solar Cells (OSCs) on Glass Substrate

## 3.1 Introduction

This study presents an extensive investigation into the fabrication and optimization of organic solar cells (OSCs) on rigid glass substrates, focusing on different device architectures and donor-acceptor interactions that influence photovoltaic (PV) performance. The research explores multiple OSC types, including:

- Bulk heterojunction (BHJ) and planar heterojunction (PHJ) OSC**s** using small molecule donors with both fullerene and non-fullerene acceptors (NFAs).
- Single-material organic solar cells (SMOSCs) based on dyad molecules with covalently linked donor-acceptor systems (D-L-A) in direct and inverted architectures.
- Homojunction organic solar cells (HOSCs) incorporating donor-π-acceptor (D-π-A) molecules in direct and inverted architectures.

Each section aims to understand how molecular design, donor-acceptor interactions, device architecture, and processing conditions affect overall PV efficiency.

## 3.2 Inverted BHJ and PHJ OSCs with Small Molecule Donors and Fullerene Acceptors

Experiments were conducted on BHJ and PHJ OSCs using different small donors and fullerene acceptor materials, deposition techniques, and optimization parameters such as thermal treatment and buffer layers.

### 3.2.1 Evaluation of Donor/Acceptor Behavior of D-A Molecules

The Molecule 7 was tested sequentially in combination with the $PC_{61}BM$ acceptor and the P3HT donor in an inverted BHJ structure (Figure 3.1).

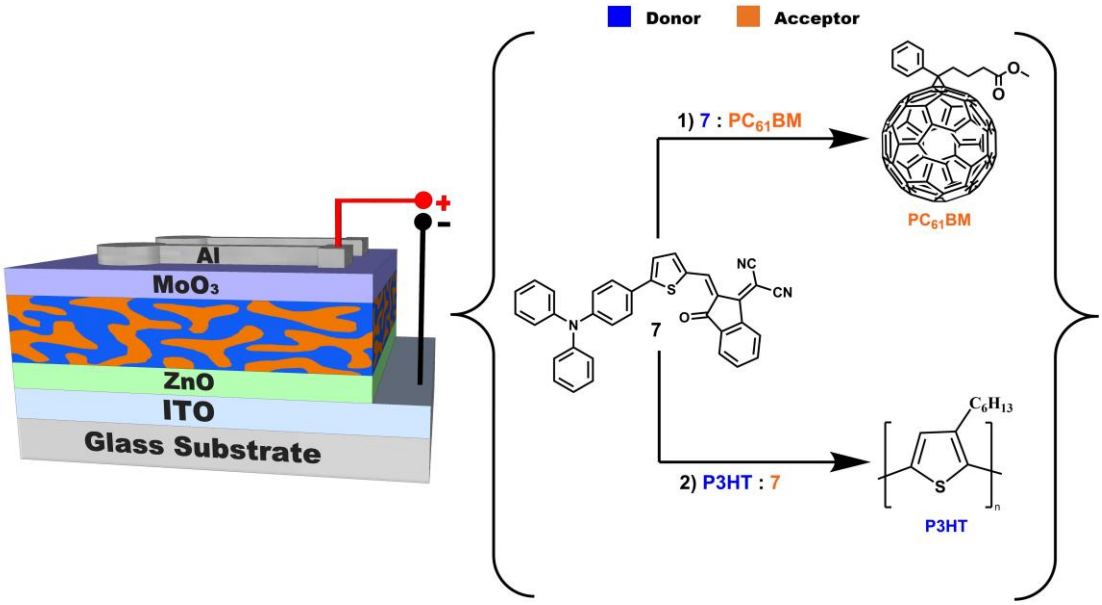


**Figure 3.1.** Inverted BHJ architecture processed from solution using two different photovoltaic blends: **7**: $PC_{61}BM$ and P3HT:**7**

In the case of the 7:PC61BM pair, the optimal donor-acceptor (D:A) ratio of 1:2 provided the highest power conversion efficiency (PCE) of 3.20%, with a short-circuit current density (Jsc) of 8.17 mA/cm² after thermal treatment at 90°C. When **7** was tested as an acceptor with P3HT as the donor, the highest PCE was 0.7% at a 1:1 ratio, suggesting its better performance as a donor.

### 3.2.2 Inverted PHJ OSCs Using Thermal Evaporation with C60 and C70 Acceptors

In an inverted bilayer architecture, donor 7 was paired with fullerene acceptors $C_{60}$ and $C_{70}$. Cells with $C_{70}$ exhibited significantly better performance (PCE of 3.24%) than those with $C_{60}$ (PCE of 1.94%), due to better absorption properties of $C_{70}$.

### 3.2.3 Investigation of D-A and A-D-A Donors with 2,2'-bi[3,2-b]thienothiophene Units

New donor molecules based on 2,2'-bi[3,2-b]thienothiophene (**8**, **9**, **10**) were tested with $PC_{61}BM$ in inverted BHJ OSCs (Figure 3.2).[25, 26]

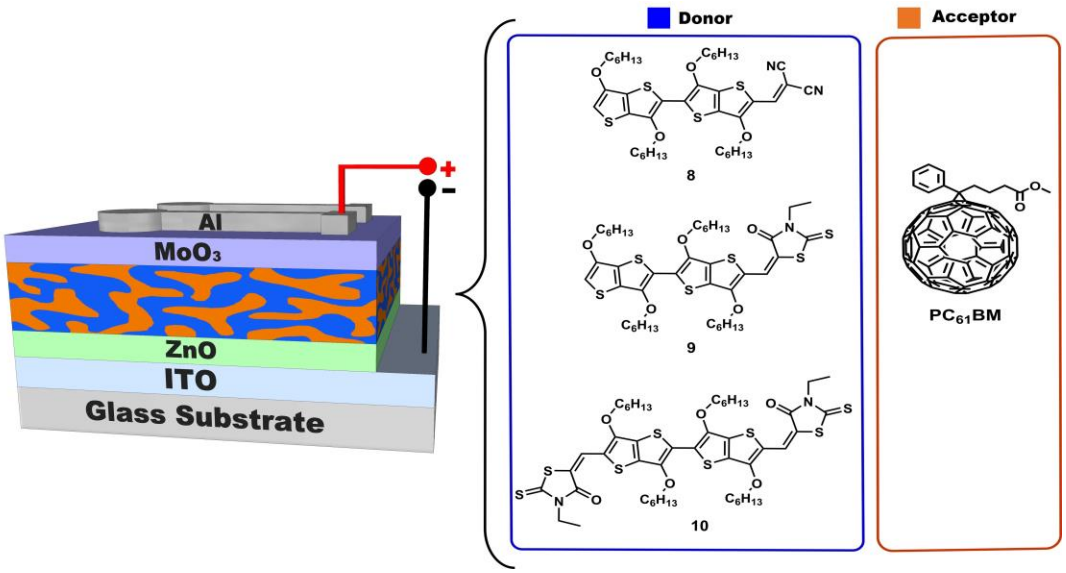


**Figure 3.2.** Architecture of inverted BHJ OSCs and the chemical structures of the active materials

Compound 10 exhibited the highest PCE of 2.50%, while compounds 8 and 9 achieved efficiencies of 0.61% and 0.57%, respectively. In PHJ structures with $C_{70}$, compounds 8 and 9 showed similar efficiency, but compound **10** degraded under vacuum conditions, limiting its applicability in PHJ architectures.[25]

### 3.2.4 Conclusions

- Molecule **7** demonstrated superior photovoltaic efficiency as a donor with $PC_{61}BM$ rather than as an acceptor with P3HT.
- $C_{70}$ was a better acceptor than $C_{60}$ in PHJ architectures.
- The novel donor **10** showed superior efficiency in BHJ structures but was unsuitable for PHJ structures due to thermal degradation.[25]

## 3.3 The Effect of Terminal Acceptor Units in Novel Non-Fullerene Acceptors

A comparative analysis of fullerene and non-fullerene acceptors (NFAs) highlighted the advantages of NFAs, including better absorption properties and improved stability. The study focused on four new A-D-A non-fullerene acceptors (11-14) with an indacenodithiophene (IDT) core and various electron-withdrawing groups (a, b, c, d).[27]

### 3.3.1 Electrochemical and Optical Properties of Indacenodithiophene Acceptors

Spectroscopic analysis revealed that modifying the electron-withdrawing terminal groups significantly affected energy levels and light absorption. The most red-shifted absorption was observed

for compound 14 (Figure 3.3), indicating stronger light absorption and better potential for photovoltaic applications.[27]

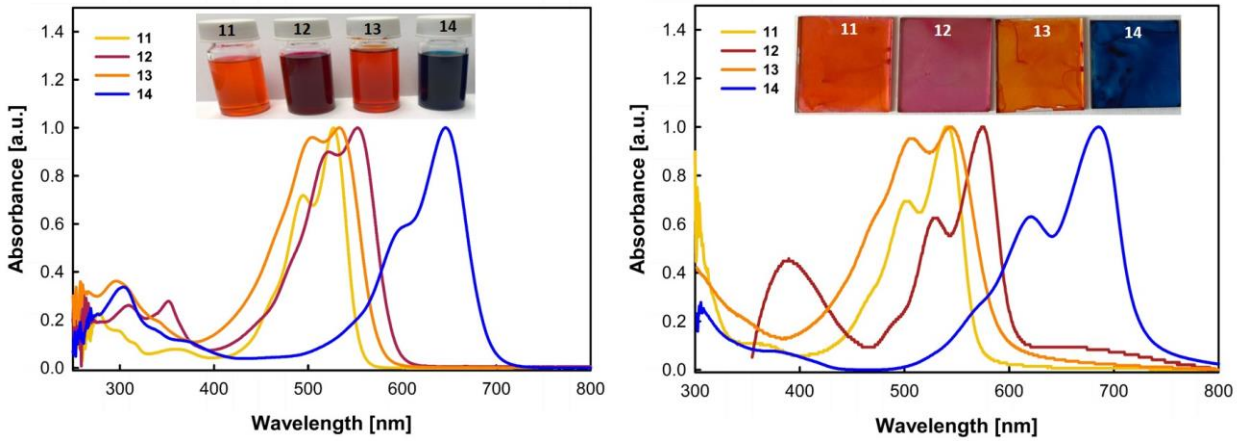


**Figure 3.3.** Normalized UV–vis absorption spectra of **11**–**14** in dichloromethane solution (left) and in thin films (right)

### 3.3.2 Fabrication and Photovoltaic Properties

P3HT was used as the donor in inverted BHJ OSCs (Figure 3.4). The best performing non-fullerene acceptors, compounds 14 (dicyanovinylindanone-based NFA) and 12 ((N-ethylrhodanine-based NFA), achieved PCEs of 2.21% and 1.74%, respectively, respectively-comparable to or better than P3HT:$PC_{61}BM$ (1.72% after annealing) when the active layer was optimized to 80 nm. Despite similar structures, the S-ethyl rhodanine-based compound 13 showed lower performance, likely due to electronic effects from tautomerization.[27]

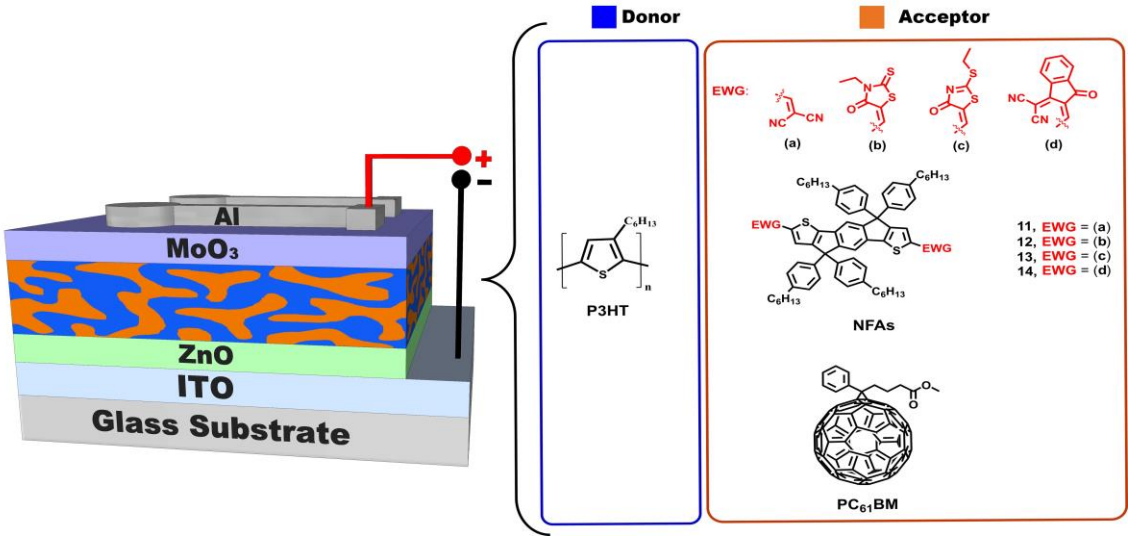


**Figure 3.4.** Inverted BHJ OSC architecture and chemical structures of the active materials

This study emphasizes the importance of selecting suitable electron-accepting groups to optimize

OSC performance, paving the way for the development of advanced n-type semiconductors with improved efficiency.[27]

## 3.4. Direct and Inverted SMOSCs Based on Arylamine and C60 Dyads

### 3.4.1 Introduction

Single-material organic solar cells (SMOSCs) offer a potential solution to the morphological instability of bulk heterojunction (BHJ) solar cells by integrating donor (D) and acceptor (A) units within a single material. Despite challenges in charge recombination and transport, SMOSCs provide advantages in simplicity and cost-effectiveness.[28, 29] Research efforts have evolved from early double-cable polymers and molecular donor-acceptor (D-A) systems to block copolymers and small molecule dyads, leading to notable improvements in power conversion efficiencies (PCEs). Recent studies have demonstrated efficiencies exceeding 14-15%, with the synthesis of novel conjugated block copolymers.[30]

This study investigates three newly synthesized dyad molecules (16, 17, and 18) based on an arylamine donor and $C_{60}$ acceptor, systematically analyzing their photovoltaic properties in both direct and inverted SMOSC architectures.[28]

### 3.4.2 Electrochemical and Optical Properties

The electrochemical properties of the three dyads were analyzed via cyclic voltammetry, estimating their HOMO-LUMO energy levels. UV-Vis spectroscopy revealed that these dyads exhibit similar electronic characteristics, with film absorption spectra displaying bathochromic shifts due to intermolecular interactions (Figure3.5). Dyad 18 showed the most significant shift and the lowest optical bandgap, indicating stronger electronic interactions within the material.[28]

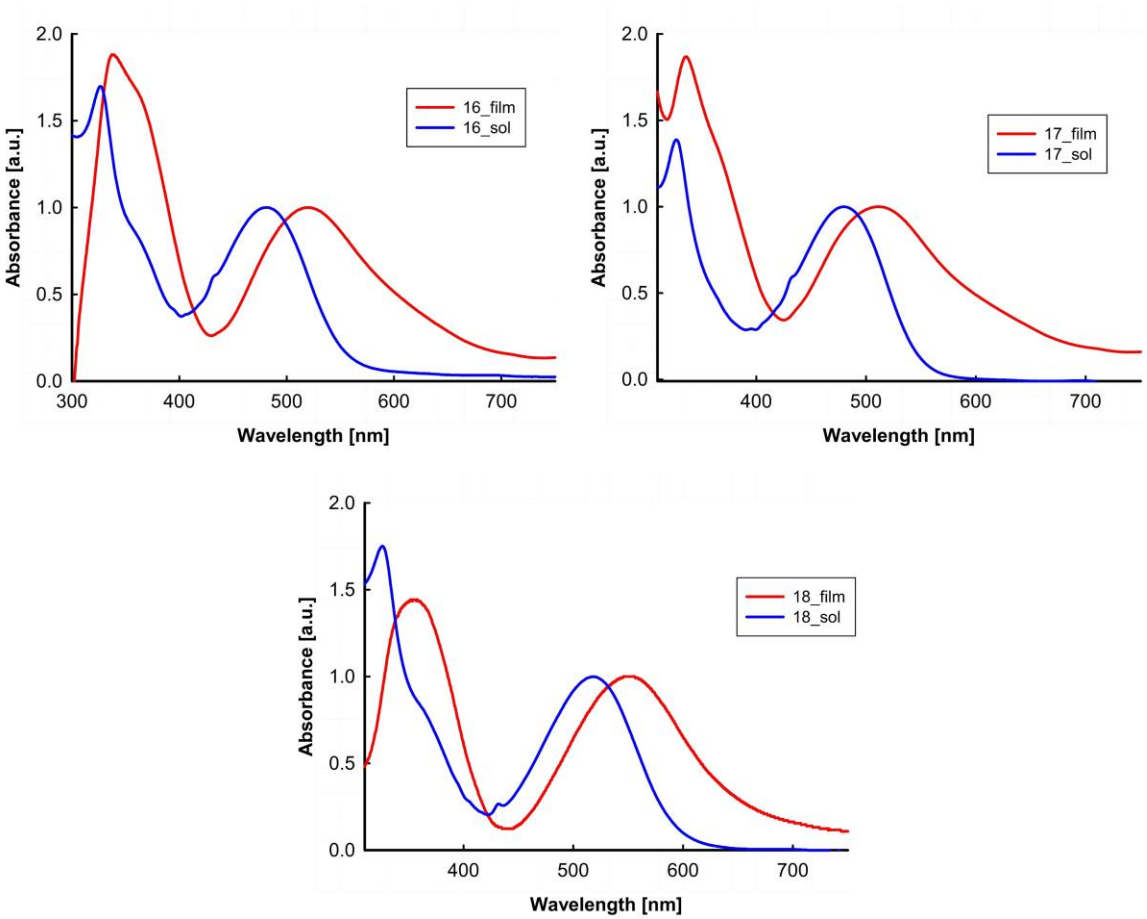


**Figure 3.5.** Normalized UV-Vis absorption spectra of **16–18** in dichloromethane solution (blue) and thin films (red)

### 3.4.3 Morphological Analysis of Active Layers

Atomic force microscopy (AFM) images demonstrated that the films formed by dyads 16 and 17 had smooth and uniform surfaces, with minimal phase segregation. In contrast, dyad 18 exhibited a less homogeneous morphology, attributed to processing difficulties arising from its molecular structure, specifically the presence of a dicyanovinyl group and a shorter alkyl linker.[28]

### 3.4.4 Fabrication and Photovoltaic Performance of SMOSCs

The photovoltaic properties of the dyads were tested in three different SMOSC architectures (Figure 3.6): **(a)**-ITO/ZnO/SM/$MoO_3$/Al, **(b)** ITO/$MoO_3$/SM/Bphen/Al, **(c)** ITO/PEDOT:PSS/SM/Al.[28]

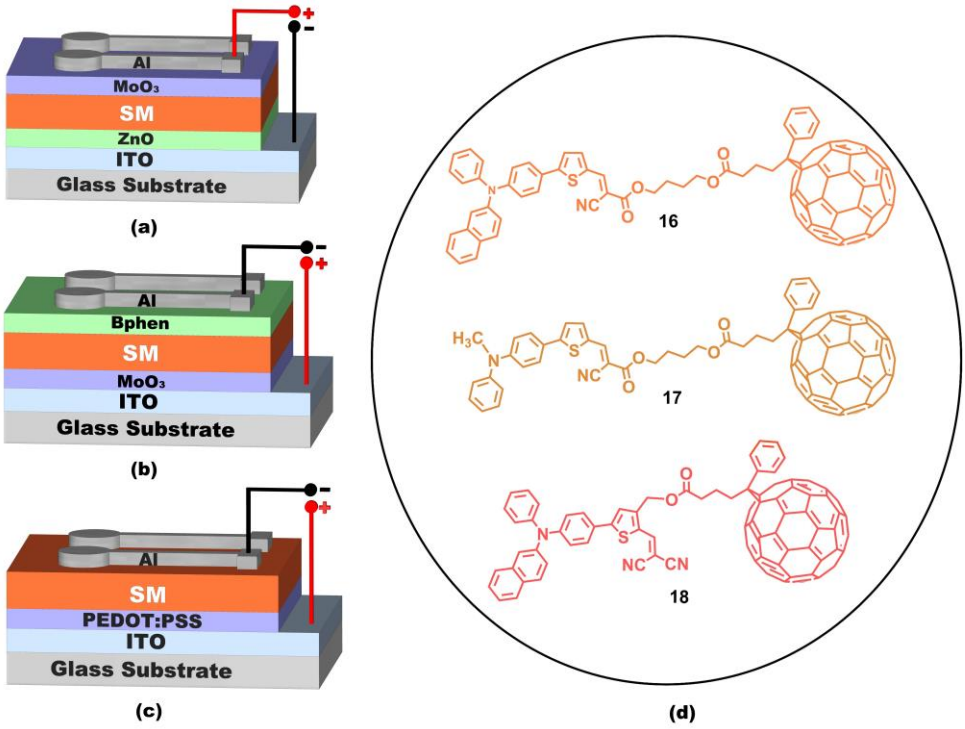


**Figure 3.6.** SMOSC architecture: (a) inverted; (b) direct with $MoO_3$ and Bphen buffer layers; (c) simple direct, and (d) chemical structures corresponding to the three dyad molecules **16**, **17**, and **18**

Optimized film thicknesses were determined to be 60 nm for dyads 16 and 17, and 50 nm for dyad 18. The inverted structure yielded the highest efficiency, with PCEs ranging from 0.8% to 0.95%. The direct structure with buffer layers achieved lower PCEs (0.57% to 0.71%), while the simple direct structure exhibited the lowest efficiencies (0.35% to 0.40%).[28]

Dyad 16, with a β-naphthyl donor and a $C_{60}$ acceptor linked at position 2 of the thiophene unit, demonstrated the best photovoltaic performance, suggesting superior charge transport properties compared to dyads 17 and 18. Despite theoretical expectations, dyad 18 exhibited lower efficiency, likely due to processability issues that led to poor film morphology and reduced charge transport.[28]

### 3.4.4 Conclusions

Dyads 16, 17, and 18, incorporating C60 and arylamine donors, showed bathochromic shifts in thin films, with 18 having the lowest bandgap but poor morphology.[28]

Among three tested SMOSC architectures, the inverted structure (a) was the most efficient (PCE: 0.8–0.95%), while direct (c) structures performed worse. Dyad 16 had the best results due to superior charge transport. Despite predictions, dyad 18 underperformed due to poor processability and charge transport issues. [28]

The findings indicate that while SMOSCs still face performance limitations compared to BHJ structures, advancements in molecular design and device architecture can significantly improve their potential for practical applications.[28]

## 3.5 Homojunction SMOSCs with Small D-A Molecules

### 3.5.1 Introduction

Small-molecule homojunction organic solar cells (HOSCs) represent a further simplification of SMOSCs.[31] Despite early challenges due to low efficiencies, recent reports suggest a resurgence of interest in this area. The key issue in HOSCs is charge generation, as exciton dissociation requires a sufficient driving force to overcome Coulomb attraction. Mechanisms such as electrode work function differences and energy disparities between molecular domains facilitate this process. [32, 33]

This section presents the first systematic analysis of small D-A molecules, consisting of triarylamine donor blocks connected to dicyanovinyl (DCV) and indanone-based acceptors (Figure 3.7). Their electrochemical and optical properties are evaluated, and their photovoltaic (PV) performance in direct and inverted architectures is discussed.[32]

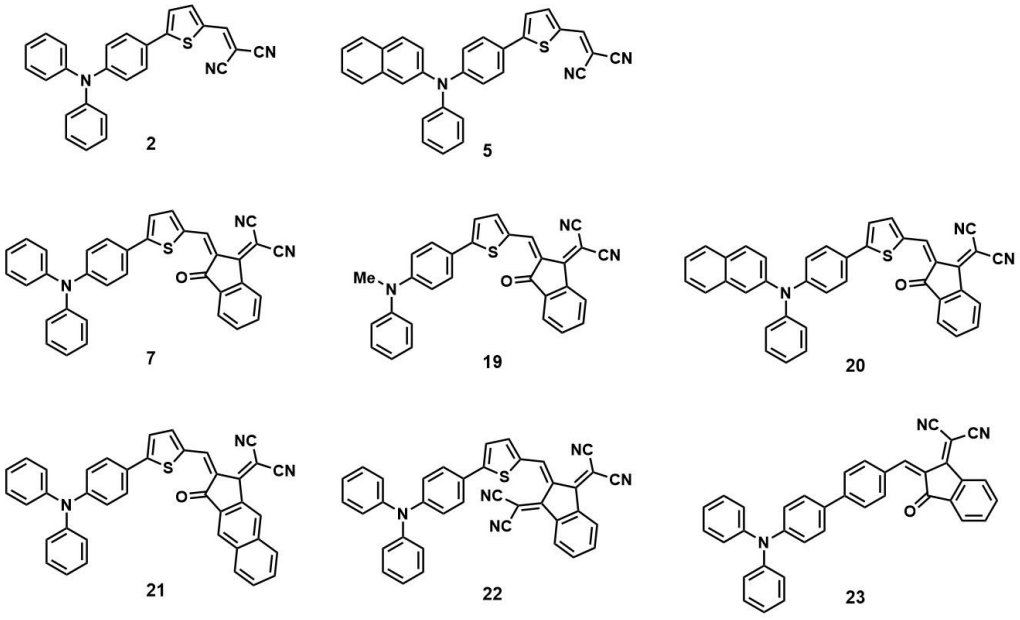


**Figure 3.7.** Chemical structures of target compounds **2, 5, 7, 19-23**

### 3.5.2 Electrochemical and Optical Properties of Active Compounds

UV-Vis spectroscopy reveals a broad absorption range for the analyzed compounds, with notable red shifts when stronger acceptor groups are introduced.[32]

The substitution of thiophene with a phenyl conjugation bridge results in a hypsochromic shift, reducing conjugation efficiency. The solid-state films exhibit bathochromic shifts and band broadening, indicating strong intermolecular interactions (Figure 3.8). The estimated band gaps range from 1.40 eV to 2.06 eV, confirming that the acceptor type significantly influences energy levels and optical properties.[32]

Cyclic voltammetry (CV) analysis shows that while the HOMO levels are primarily determined by the arylamine donor block, the LUMO levels and overall energy gaps are governed by the acceptor strength and conjugation bridge. Theoretical calculations align well with experimental data, validating these trends.[32]

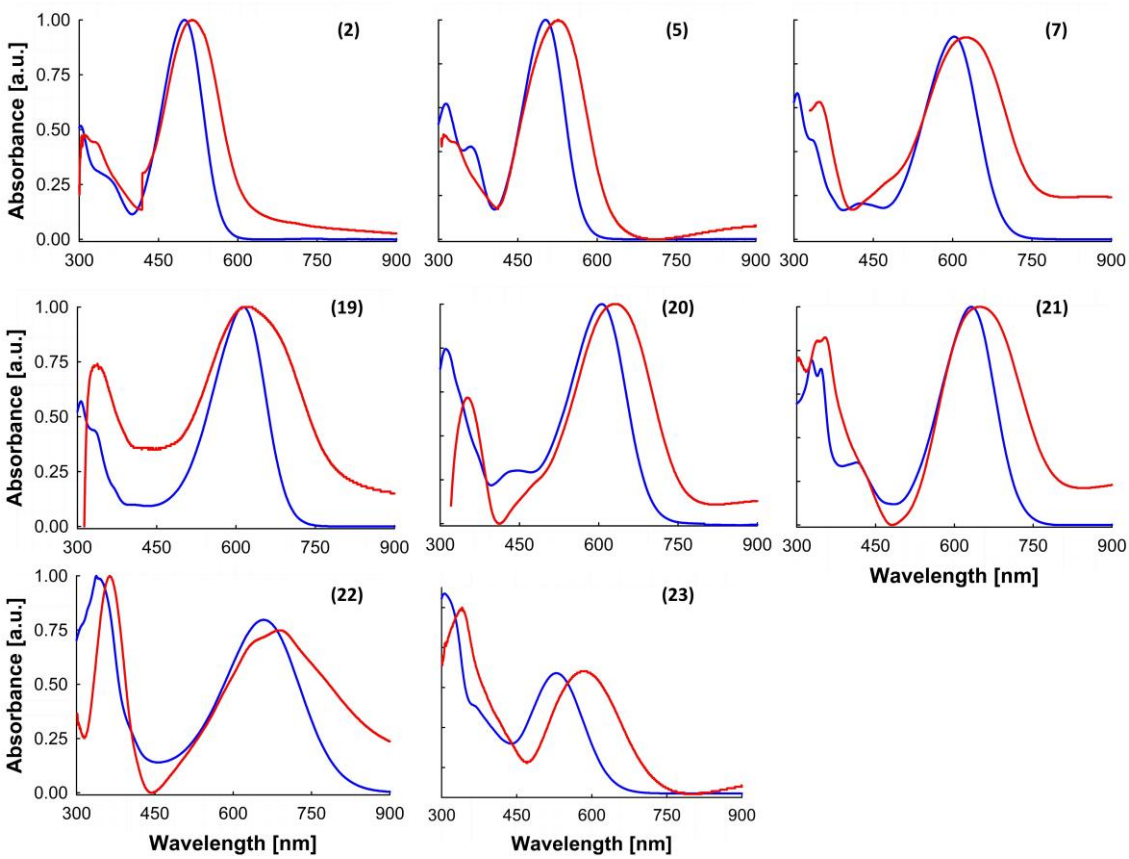


**Figure 3.8.** Normalized UV/Vis absorption spectra of compounds **2**, **5**, **7**, **19–23**. Blue lines: in dichloromethane (DCM) solution. Red lines: thin films obtained by spin-casting on glass from chloroform solutions

### 3.5.3 Fabrication and Photovoltaic Properties of SMOSCs

The PV performance of compounds **2, 5, 7, 19–23** was evaluated in both direct (ITO/$MoO_3$/SM/Bphen/Al) and inverted (ITO/ZnO/SM/$MoO_3$/Al) architectures (Figure 3.9), using thermal evaporation to deposit active layers.[32]

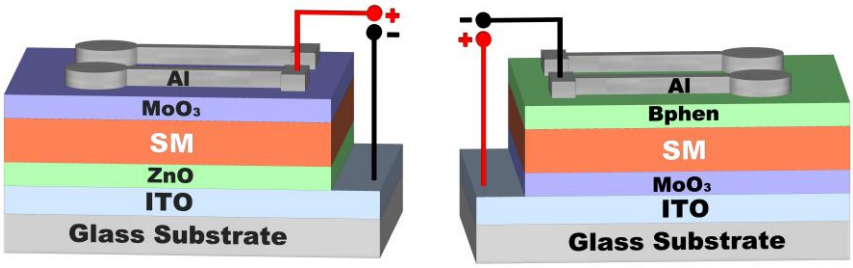


**Figure 3.9.** HOSC architecture in inverted (left) and direct (right) configurations

Optimization revealed that a 20 nm thickness provided the highest efficiency for compound **7**, achieving a PCE of 0.86% and a Jsc of 3.49 mA/cm² in the inverted structure.

Comparing direct and inverted architectures, the latter consistently exhibited twice the Jsc and PCE values due to superior charge transport facilitated by ZnO and $MoO_3$ layers. Compounds **7 and 20** showed the best performance, with **PCE ~0.9%** and **Jsc ~3.5 mA/cm²** in inverted cells, and **PCE ~0.5%** in direct cells (Figure 3.10). The EQE spectra corroborated these findings, with peak EQE values reaching ~23% in inverted cells for this two compounds (Figure 3.11).[32]

S**tructural Modifications:**

- Replacing the phenyl donor group with β-naphthyl (compound **5**) or a methyl group (compound **19**) did not enhance efficiency.[32]
- Substituting DCV acceptors (used in compounds **2** and **5**) with dicyanovinylindandione units (compounds **7** and **20**) doubled PCE and Jsc, demonstrating the critical role of acceptor strength in charge separation.[32]
- Replacing the thiophene bridge with a phenyl bridge (compound **23**) resulted in reduced conjugation and lower intramolecular charge transfer (ICT) intensity, leading to decreased performance.[32]
- Attempts to further enhance acceptor strength (as in compound **22**, with a bis(dicyanovinyl)indandione unit) led to lower efficiencies, likely due to processability challenges and limited molecular organization.[32]

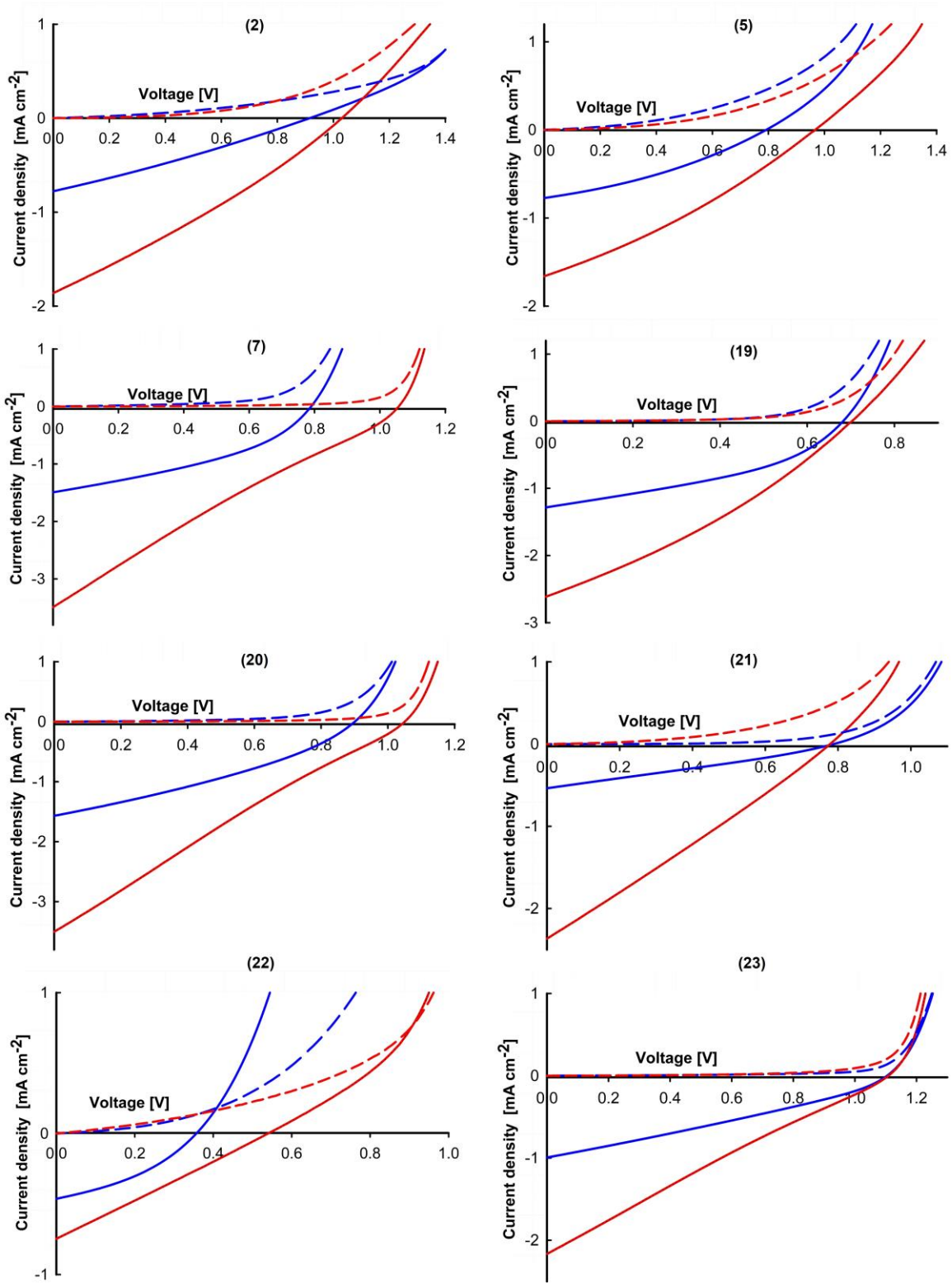


**Figure 3.10.** Current density vs. voltage curves for the direct (blue) and inverted (red) cells based on compounds **2**, **5**, **7**, **19**–**23**, processed via thermal evaporation under high vacuum. Dashed lines: in the dark; solid lines: under simulated AM 1.5 solar illumination

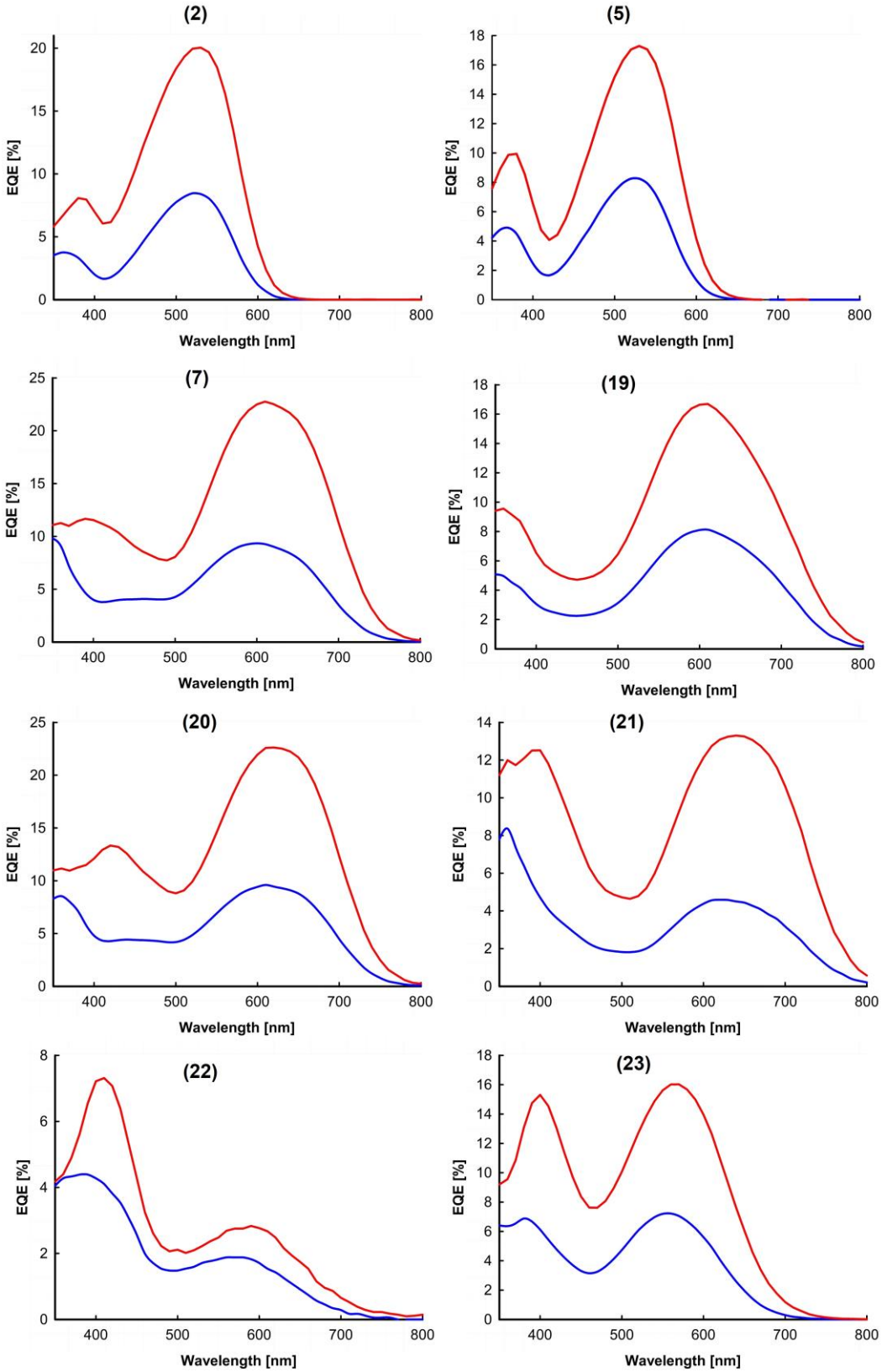


**Figure 3.11.** External quantum efficiency (EQE) spectra for the inverted (red) and direct (blue) cells based on compounds **2**, **5**, **7**, **19**–**23**

### 3.5.4 Conclusions

This section analyzed eight small D-A molecules, showing that the bandgap can be tuned

by ~0.70 eV through acceptor and conjugation bridge modifications. Compounds 7 and 20 were the most efficient, reaching PCE ~0.9% in inverted and ~0.5% in direct HOSCs. Compound 21, when deposited via solution processing, performed similarly to 7 and 20 but degraded under thermal evaporation. The active layer thickness was optimized at 20 nm for maximum performance.[32]

Replacing the DCV acceptor with dicyanovinylindandione (7, 20) doubled efficiency, while other modifications had limited impact due to processability issues. Despite PCE <1%, these molecules offer low cost, stability, and simple architecture, making them promising for further organic photovoltaic research. Future work should focus on structural and device optimizations to improve performance.[32]

## 3.6 Chapter's Conclusions

This chapter highlights the strong correlation between the chemical structure of organic compounds and their electrochemical, optical, and photovoltaic properties, offering insights into optimizing OSC performance on glass substrates.

- Compound 7 exhibits both donor and acceptor behavior, with a stronger donor tendency, demonstrating the importance of tuning donor-acceptor balance for improved OSC efficiency.
- A-D-A conjugated systems with an IDT-based backbone showed that electron-accepting groups significantly influence energy levels and absorption. Dicyanovinylindanone and N-ethylrhodanine were the most promising acceptors, achieving efficiencies comparable to P3HT:$PC_{61}BM$.[27]
- Arylamine-fullerene dyads in SMOSCs confirmed that inverted architectures (ITO/ZnO/SM/$MoO_3$/Al) outperform direct ones, with Dyad 16 reaching PCE ~1%.[28]
- HOSCs with small D-A molecules showed that compounds **7** and **20** achieved the highest efficiency due to a dicyanovinylindandione acceptor, but performance remained below 1%. The inverted HOSC architecture proved superior, reinforcing the importance of optimized charge transport layers.[32]

These findings emphasize the impact of molecular design, donor-acceptor interactions, and device architecture on OSC performance. Further research should focus on improving small-molecule-based organic photovoltaics, particularly SMOSCs, where efficiency enhancement remains a major challenge.[33]

# Chapter 4: Investigation of Novel OSCs on Flexible PET Substrate

## 4.1 Introduction

This chapter explores organic solar cells (OSCs) on flexible polyethylene terephthalate (PET) substrates, highlighting their advantages such as low-cost fabrication, mechanical flexibility, lightweight design, and scalability.[34] While PCE improvements on flexible substrates lag behind rigid ones, their adaptability makes them ideal for applications in building-integrated photovoltaics, wearable electronics, and autonomous devices like drones. [35, 36] The research explores:

- Comparative performance analysis of BHJ and PHJ OSCs on glass vs. PET substrates using compound **20** as the donor.
- Development of SMOSCs on flexible substrates, including heterojunction (dyads 16, 17) and homojunction (small molecules 2, 7, 20) architectures. [37]
- Scalability and application testing, examining cell size effects, series/parallel connections, and real-world applications such as powering LEDs and charging supercapacitors for body sensors.

## 4.2 Comparison of BHJ and PHJ OSCs on PET vs. Glass

### 4.2.1 Inverted and Direct BHJ OSCs

The study analyzed **Compound 20**, a donor-acceptor (D-A) molecule, in BHJ inverted structure combined with **$PC_{61}BM$** acceptors (Figure 4.1). On rigid glass, BHJ OSCs achieved a **PCE of 2.71% (inverted) and 2.09% (direct)**, but on PET, efficiency dropped by ~20% to **2.2% (inverted) and 1.61% (direct)** due to:

- Higher sheet resistance of PET-ITO (60 Ω/sq vs. 10 Ω/sq for glass-ITO), leading to increased series resistance (Rs).
- Increased surface roughness (RMS ~5 nm for PET vs. 1-2 nm for glass), affecting charge transport and film uniformity.

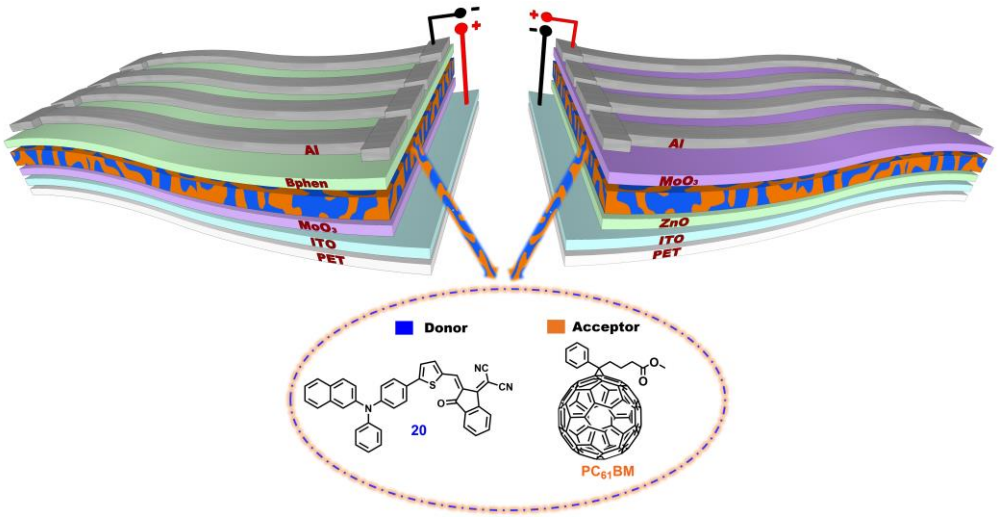


**Figure 4.1.** Direct (left) vs. Inverted (right) BHJ architecture on PET Substrate

- Lower transmittance of PET (~80% at 550 nm vs. ~89% for glass), reducing light absorption.

### 4.2.2 Inverted and Direct PHJ OSCs

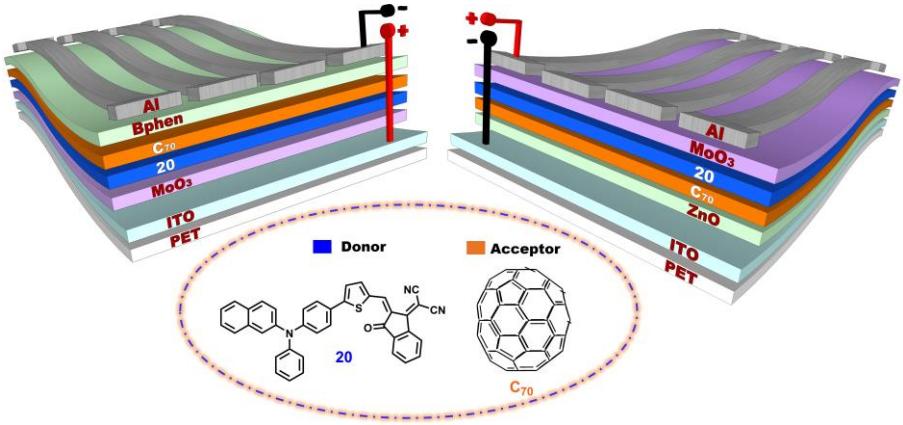


**Figure 4.2.** Direct (left) vs Inverted (right) PHJ architecture on PET Substrates

For PHJ architectures (Figure 4.2) using $C_{70}$ as the acceptor and compound **20** as donor , OSCs on PET exhibited even greater efficiency losses (~30%) than those on glass:

- On glass: PCE of 2.53% (inverted) and 1.16% (direct).
- On PET: PCE dropped to 1.78% (inverted) and 0.80% (direct).
- The increased losses in PHJ structures on PET were attributed to surface roughness, uneven film thickness, recombination losses, and reduced charge extraction caused by PET's lower thermal conductivity.
- Despite these losses, optimized deposition conditions can improve PHJ film uniformity on larger areas, highlighting the potential for scalable OSC arrays and the need for tailored fabrication

strategies for flexible substrates.

## 4.3 Design, Fabrication, and Characterization of Flexible Single Material Organic Solar Cells (SMOSCs)

This section investigates single-material organic solar cells (SMOSCs) on flexible PET substrates, comparing their performance to rigid glass substrates. The study explores both heterojunction (dyads 16, 17) and homojunction (2, 7, 20) architectures using direct and inverted configurations (Figure 4.3).[37]

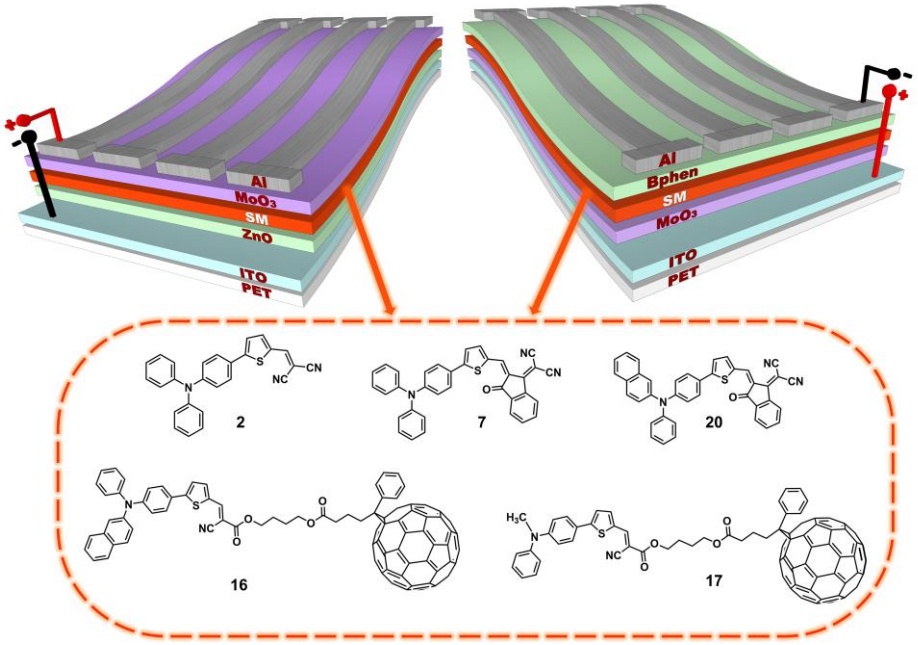


**Figure 4.3.** Inverted architecture (left) vs. direct architecture (right) of SMOSCs on PET substrate

**Fabrication & Device Performance**:

- Heterojunction SMOSCs (16, 17) performed best, with compound 16 achieving the highest efficiency at 0.83% (inverted) and 0.43% (direct), while compound 17 showed slightly lower performance (Table 4.1).[37]

**Table 4.1.** Solar simulator results for SMOSCs based on dyadic molecules on PET vs. glass substrate

| Cell Type | Compd | Substrate | Voc (V) | Jsc (mA/cm2) | FF (%) | PCE (%) | Rs (Ω) | Rp (Ω) |
|---|---|---|---|---|---|---|---|---|
| Direct | **16** | glass | **1.06** | **2.34** | **28.58** | **0.71** (0.67) | 714.38 | 1979.17 |
| | | PET | **1.00** | **1.60** | **26.92** | **0.43** (0.40) | 1567.04 | 2471.45 |
| | **17** | glass | **0.92** | **2.14** | **29.66** | **0.59** (0.56) | 646.18 | 1980.76 |
| | | PET | **0.94** | **1.71** | **26.37** | **0.42 (**0.39) | 1333.04 | 2205.95 |

| | | | | | | | | |
|---|---|---|---|---|---|---|---|---|
| Inverted | **16** | glass | **1.01** | **3.03** | **31.23** | **0.95** (0.91) | 543.82 | 1941.78 |
| | | PET | **1.00** | **2.79** | **29.86** | **0.83** (0.77) | 696.98 | 1827.79 |
| | **17** | glass | **0.91** | **2.95** | **30.90** | **0.83** (0.80) | 463.15 | 1596.12 |
| | | PET | **0.92** | **2.20** | **35.57** | **0.72** (0.64) | 691.53 | 3856.75 |

- Homojunction OSCs (2, 7, 20) followed a similar trend, with compounds 7 and 20 reaching 0.46% (inverted) and ~0.2% (direct) (Tabele 4.2).[37]

**Table 4.2.** Solar simulator results for HOSCs on PET vs. glass substrates

| Cell Type | Compd | Substrate | Voc (V) | Jsc ($mA/cm^2$) | FF (%) | PCE (%) | Rs (Ω) | Rp (Ω) |
|---|---|---|---|---|---|---|---|---|
| Direct | **2** | glass | **0.91** | **0.78** | **28.0** | **0.20** (0.18) | 3405.95 | 5218.73 |
| | | PET | **0.84** | **0.60** | **26.48** | **0.13** (0.12) | 4547.64 | 5623.14 |
| | **7** | glass | **0.73** | **1.49** | **33.9** | **0.46** (0.42) | 530.03 | 3685.51 |
| | | PET | **0.97** | **1.01** | **23.18** | **0.23** (0.21) | 2795.61 | 3157.56 |
| | **20** | glass | **0.90** | **1.57** | **33.7** | **0.48** (0.45) | 785.98 | 3373.45 |
| | | PET | **0.76** | **0.82** | **28.69** | **0.18** (0.17) | 2345.33 | 4135.21 |
| Inverted | **2** | glass | **1.03** | **1.86** | **28.91** | **0.55** (0.50) | 1335.95 | 2534.25 |
| | | PET | **0.77** | **1.34** | **30.27** | **0.31** (0.27) | 1383.83 | 2852.62 |
| | **7** | glass | **1.05** | **3.49** | **23.6** | **0.86** (0.82) | 543.73 | 987.55 |
| | | PET | **0.87** | **2.10** | **25.0** | **0.46** (0.42) | 1398.06 | 1459.50 |
| | **20** | glass | **1.03** | **3.50** | **24.1** | **0.87** (0.83) | 627.35 | 1093.69 |
| | | PET | **0.98** | **1.80** | **26.10** | **0.46** (0.42) | 1506.60 | 2207.51 |

- Inverted architectures outperformed direct ones, showing higher PCE due to improved charge transport and reduced series resistance (Rs).[37]

**Substrate Effects:**

- Solution-processed dyad-based SMOSCs showed a lower efficiency drop (~10-30%) on PET.[37]
- Thermally evaporated HOSCs suffered greater efficiency losses (~40-50%) due to PET's higher roughness and lower thermal conductivity, leading to increased charge recombination.[37]
- The thin active layers (20 nm) of HOSCs were more sensitive to substrate defects, further

affecting charge transport.[37]

Despite lower efficiency on PET substrates, the optimized deposition methods provide a cost-effective, scalable approach for flexible photovoltaic applications. The high transparency of HOSCs makes them particularly promising for smart window technologies and lightweight energy solutions.[37]

## 4.4 Design, Fabrication, and Utilization of Series/Parallel Connected Flexible OSC Arrays for Low-Power Devices

This section focuses on the design, fabrication, and application of flexible organic solar cell (OSC) arrays on PET substrates, aiming to enhance voltage (Voc) and current (Isc) output for powering low-power electronics.

**Electrical Parameters:**

-An individual OSC cell (28 $mm^2$) with compound 20 was tested in previous sections in inverted BHJ, PHJ, and SMOSC configurations, with BHJ providing the highest Isc (1.8 mA).

- The inverted PHJ structure (ITO/ZnO/$C_{70}$/20/$MoO_3$/Al), which had an Isc of 1.2 mA, was selected for array fabrication due to its higher reproducibility and lower risk of short circuits on large PET substrates

**Parallel and Series-Connected OSC Arrays:**

- Two 3D-printed masks were designed to fabricate single and parallel-connected OSC arrays, improving current output.
- **Mask 1**: Used for the fabrication of individual cells and parallel connections, analyzing the effect of the organic layer deposition area on the PET substrate.
- **Mask 2** (Figure 4.4): Enabled six cell arrays (four OSCs per array) connected in parallel, allowing for a fourfold increase in Isc while maintaining Voc scalability through series connections.

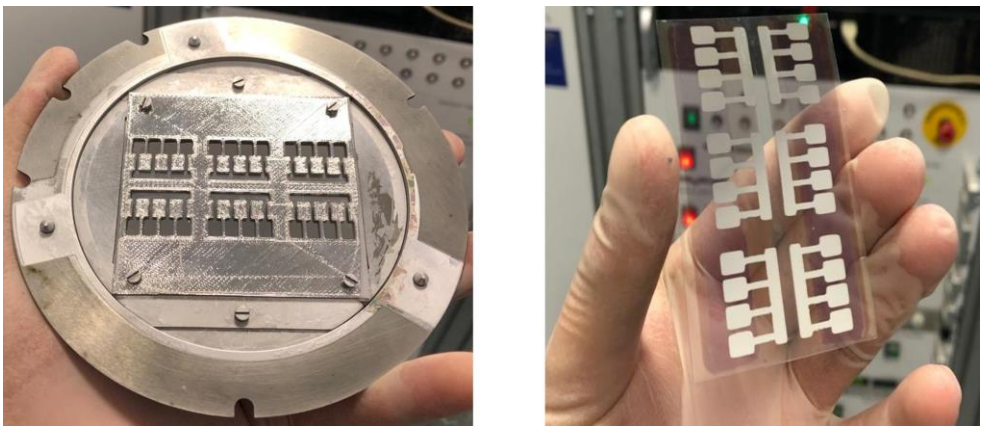

**Figure 4.4**. Mask 2 mounted on the evaporation support (left) and the final PET cell (right)

**Performance of OSC Arrays:**

- The best-performing series-connected OSC arrays (four arrays in series) provided Voc = 3.6 V and Isc = 2.2 mA under AM 1.5 solar illumination.
- This array successfully powered red, green, and blue LEDs, demonstrating its potential as a lightweight flexible energy source (Figure 4.5).

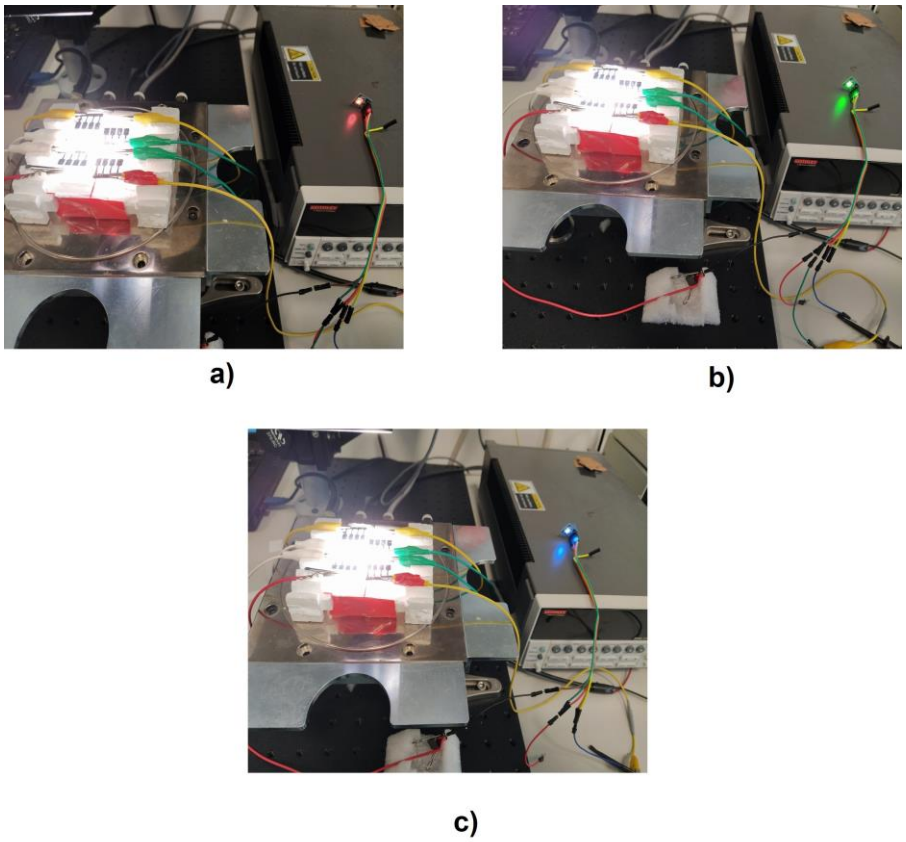


**Figure 4.5.** Activation of LEDs: red (a), green (b), and blue (c) with four cell arrays connected in series

**Supercapacitor Charging Experiment:**

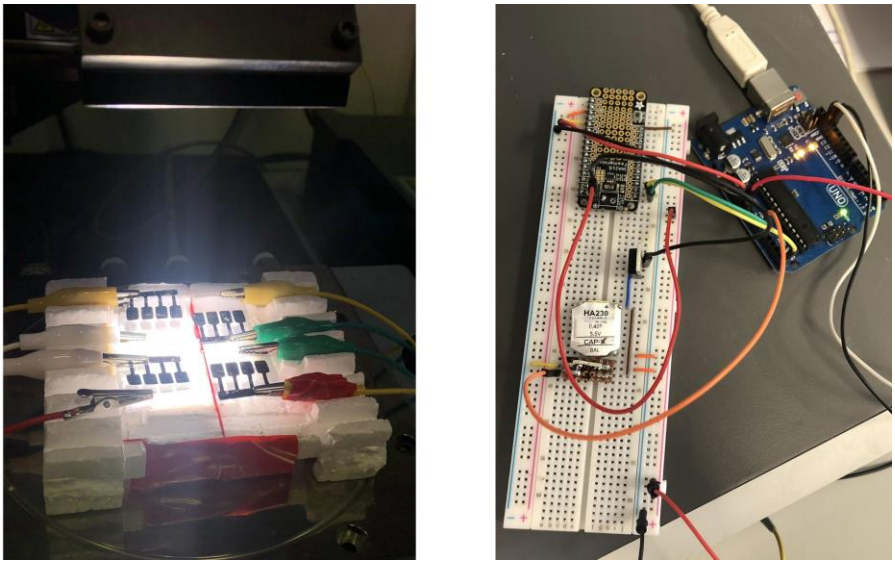

**Figure 4.6.** Testing the charging of the HA230 0.4F/5.5V supercapacitor in an on-body sensor system prototype from four series-connected OSC arrays on PET

- The OSC array was tested for charging a HA230 (0.4F/5.5V) supercapacitor in an on-body sensor system (Figure 4.6).[38]
- The setup required 24 minutes to reach 3V (Figure 4.7), longer than the theoretical approximately 10 minutes, due to electrical losses and OSC operating conditions.

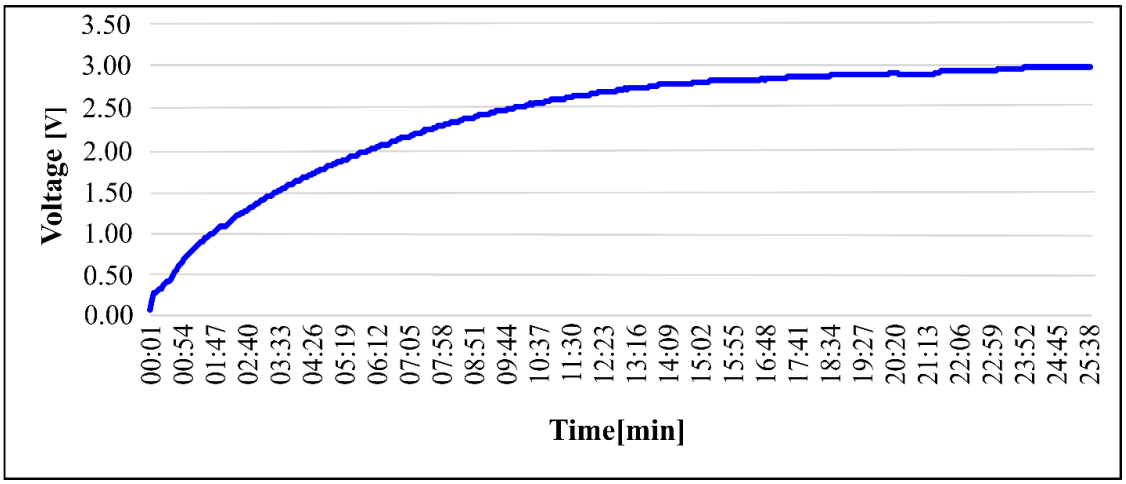


**Figure 4.7.** Charging the supercapacitor using four series-connected PHJ inverted OSC arrays on a PET substrate

- Future improvements should focus on optimizing electrical connections to reduce losses and improve efficiency

## 4.5 Chapter's Conclusions

This chapter analyzed the impact of design, fabrication, and optimization on the performance of OSC architectures on PET substrates and their application in low-power electronics.

-BHJ OSCs adapted better to PET than PHJ OSCs, where substrate roughness caused higher efficiency losses. However, deposition optimization can improve PHJ uniformity for large-area applications.

-SMOSCs: Heterojunction-based structures retained efficiency better on PET than homojunction-based ones, which were more affected by substrate roughness due to thinner active layers and deposition methods. Despite performance losses, HOSCs remain promising for lightweight and transparent photovoltaic applications.[37]

-Practical Integration: Flexible OSC arrays successfully powered LEDs and charged a supercapacitor for an on-body sensor, demonstrating their feasibility for wearable and low-power electronics.

Future Research: Efforts should focus on improving interconnections, reducing power losses, and exploring alternative flexible substrates to enhance performance and reliability.

# General Conclusions

This thesis explored the development and optimization of heterojunction and homojunction organic solar cells (OSCs), assessing how device architecture, fabrication techniques, and molecular design influence photovoltaic performance. Key optimization strategies, including thermal treatment, solvent selection, and donor-acceptor tuning, significantly improved OSC efficiency, with inverted structures proving superior to direct ones in terms of stability and charge transport.

Studies on glass substrates confirmed the advantages of non-fullerene acceptors (NFAs) and demonstrated the feasibility of single-material OSCs (SMOSCs) and homojunction OSCs (HOSCs), with dicyanovinylindandione derivatives emerging as the most efficient in HOSCs. Research on flexible PET substrates highlighted their potential for wearable and low-power applications, with BHJ OSCs adapting better than PHJ OSCs. Flexible OSC arrays successfully powered LEDs and charged supercapacitors, showcasing their practical viability.

This research contributed to the advancement of OSC technology with 9 journal publications, 2 patents, and 3 conference presentations, laying the foundation for future optimizations and the development of new organic materials to enhance OSC performance on both rigid and flexible substrates.

# Bibliograpy


(1) E. K. Solak and E. Irmak, *RSC Adv.*, 2023, **13**, 12244–12269.

(2) H. Chen, Y. Huang, R. Zhang, H. Mou, J. Ding, J. Zhou, Z. Wang, H. Li, W. Chen, J. Zhu, Q. Cheng, H. Gu, X. Wu, T. Zhang, Y. Wang, H. Zhu, Z. Xie, F. Gao, Y. Li and Y. Li, *Nat. Mater.*, 2025, **24**, 444–453.

(3) L. Meng, Y. Zhang, X. Wan, C. Li, X. Zhang, Y. Wang, X. Ke, Z. Xiao, L. Ding,

R. Xia, H.-L. Yip, Y. Cao and Y. Chen, Science, 2018, **361**, 1094–1098.

(4) W. Tress, *Organic Solar Cells: Theory, Experiment, and Device Simulation*, Springer International Publishing, 2014.

(5) V. Petrova-Koch, in *High-Efficient Low-Cost Photovoltaics: Recent Developments*, Springer Berlin Heidelberg, 2009, pp. 1–5.

(6) C. W. Tang, *Appl. Phys. Lett.*, 1986, **48**, 183–185.

(7) L. Zhu, M. Zhang, J. Xu, C. Li, J. Yan, G. Zhou, W. Zhong, T. Hao, J. Song, X. Xue, Z. Zhou, R. Zeng, H. Zhu, C.-C. Chen, R. C. I. MacKenzie, Y. Zou, J. Nelson, Y. Zhang, Y. Sun and F. Liu, *Nat. Mater.*, 2022, **21**, 656–663.

(8) P. Kumaresan, S. Vegiraju, Y. Ezhumalai, S. L. Yau, C. Kim, W.-H. Lee and M.-C. Chen, *Polymers*, 2014, **6**, 2645–2669.

(9) A. Labrunie, PhD thesis, Université d'Angers, 2017.

(10) D. Kearns and M. Calvin, *J. Chem. Phys.*, 1958, **29**, 950–951.

(11) W. Cao and J. Xue, *Energy Environ. Sci.*, 2014, **7**, 2123–2144.

(12) C. Anrango-Camacho, K. Pavon-Ipiales, B. A. Frontana-Uribe and A. Palma-Cando, *Nanomaterials*, 2022, **12**, 443.

(13) N. L. T. Ameri and C. J. Brabec, *Energy Environ. Sci.*, 2013, **6**, 2390–2413.

(14) S. S. N. Chander and S. S. K. Iyer, *Sol. Energy Mater. Sol. Cells*, 2017, **161**, 407–415.

(15) G. Li, W. Li, X. Guo, B. Guo, W. Su, Z. Xu and M. Zhang, *Org. Electron.*, 2019, **64**, 241–246.

(16) T. Paula and M. de F. Marques, *AIMS Energy*, 2022, **10**, 149–176.

(17) D. Hu, Q. Yang, H. Chen, F. Wobben, V. M. L. Corre, R. Singh, T. Liu, R. Ma, H. Tang, L. J. A. Koster, T. Duan, H. Yan, Z. Kan, Z. Xiao and S. Lu, *Energy Environ. Sci.*, 2020, **13**, 2134–2141.

(18) Y. Liang, Z. Xu, J. Xia, S.-T. Tsai, Y. Wu, G. Li, C. Ray and L. Yu, *Adv. Mater.*, 2010, **22**, E135–E138.

(19) D. Deng, Y. Zhang, J. Zhang, Z. Wang, L. Zhu, J. Fang, B. Xia, Z. Wang, K. Lu, W. Ma and Z. Wei, *Nat. Commun.*, 2016, **7**, 13740.

(20) J. Huang, J. Fu, B. Yuan, H. Xia, T. Chen, Y. Lang, H. Liu, Z. Ren, Q. Liang, K. Liu, Z. Guan, G. Zou, H. T. Chandran, T. W. B. Lo, X. Lu, C.-S. Lee, H.-L. Yip, Y.-K. Peng and G. Li, *Nat. Commun.*, 2024, **15**, 10565.

(21) G. I. Giurgi, L. Szolga, I. Kovacs, E. Bogdan, N. D. Hădade, A. Terec, I. Grosu and J. Roncali, *Stud. Univ. Babeș-Bolyai Chem.*, 2020, **65**, 95–106.

(22) N. Terenti, G.-I. Giurgi, L. A. Szolga and I. Grosu, *Patent*, RO 134664 B1, 2023.

(23) G.-I. Giurgi, L. Szolga, I. Kovacs, E. Bogdan, N. D. Hădade, A. Terec, I. Grosu and J. Roncali, *Stud. Univ. Babeș-Bolyai Chem.*, 2021, **66**, 97–105.

(24) G.-I. Giurgi, L. Szolga, A. Bogdan, A. P. Crișan and I. Grosu, *Patent Application*, A/00469, 2022.

(25) L. Gabrian, G. I. Giurgi, L. Szolga, A. P. Crișan, E. Bogdan, R. Gălătuș, A. Terec and I. Grosu, *Stud. Univ. Babeș-Bolyai Chem.*, 2023, **68**, 275–283.

(26) L. Gabrian, G. I. Giurgi, I. Stroia, E. Bogdan, A. P. Crișan, N. D. Hădade, I. Grosu and A. Terec, *Molecules*, 2022, **27**, 8463.

(27) N. Terenti, G. I. Giurgi, L. Szolga, I. Stroia, A. Terec, I. Grosu and A. P. Crișan, *Molecules*, 2022, **27**, 1229–1244.

(28) A. Bogdan, L. Szolga, G. I. Giurgi, A. P. Crișan, D. Bogdan, S. Hadsadee, S. Jungsuttiwong, R. Po, I. Grosu and J. Roncali, *Dyes Pigm.*, 2021, **184**, 108845.

(29) M. I. Nan, E. Lakatos, G.-I. Giurgi, L. Szolga, R. Po, A. Terec, S. Jungsuttiwong, I. Grosu and J. Roncali, *Dyes Pigm.*, 2020, **181**, 108527.

(30) Y. Cheng, B. Huang, Q. Mao, X. Huang, J. Liu, C. Zhou, W. Zhou, X. Ren, S. Kim, W. Kim, Z. Sun, F. Wu, C. Yang and L. Chen, *Adv. Mater.*, 2024, **36**, 2312938.

(31) J. Roncali, *Adv. Energy Mater.*, 2021, **11**, 2102987.

(32) N. Terenti, G.-I. Giurgi, A. P. Crișan, C. Anghel, A. Bogdan, A. Pop, I. Stroia, A. Terec, L. Szolga, I. Grosu and J. Roncali, *J. Mater. Chem. C*, **2022**, *10*, 5716–5726.

(33) D.-F. Bogoșel, G.-I. Giurgi, A. Balan, A. Pop, I. Grosu, A. P. Crișan and A. Terec, *Org. Electron.*, **2025**, *141*, 107212.

(34) Q. Wang, Z. Na, L. Yu, S. Dai, M. K. Nazeeruddin and H. Yang, *Adv. Sci.*, **2024**, *11*, 2407177.

(35) R. Liu, Z. L. Wang, K. Fukuda and T. Someya, *Nat. Rev. Mater.*, **2022**, *7*, 870–886.

(36) B. Hailegnaw, S. Demchyshyn, C. Putz, L. E. Lehner, F. Mayr, D. Schiller, R. Pruckner, M. Cobet, D. Ziss, T. M. Krieger, A. Rastelli, N. S. Sariciftci, M. C. Scharber and M. Kaltenbrunner, *Nat. Energy*, **2024**, *9*, 677–690.

(37) G.-I. Giurgi, N. Terenti, A. P. Crișan, A. Terec, R. Gălătuș, L. Szolga and I. Grosu, *In preparation*.

(38) L. A. Szolga and T. M. Girbovan, *J. Phys.: Conf. Ser.*, **2021**, *2016*, 012004.

# List of publications

**1. Structure-properties of small donor-acceptor molecules for homojunction single-material organic solar cells**

Natalia Terenti[†], **Gavril-Ionel Giurgi**[†], Andreea Petronela Crișan, Cătălin Anghel, Alexandra Bogdan, Alexandra Pop, Ioan Stroia, Anamaria Terec, Lorant Szolga, Ion Grosu, Jean Roncali

*Journal of Materials Chemistry C*, 2022, **10**, 5716-5726.

[†] These authors contributed equally to this work.

**2. Effect of the Terminal Acceptor Unit on the Performance of Non-Fullerene Indacenodithiophene Acceptors in Organic Solar Cells**

Natalia Terenti[†], **Gavril-Ionel Giurgi**[†], Lorant Szolga, Ioan Stroia, Anamaria Terec, Ion Grosu, Andreea Petronela Crișan

*Molecules*, 2022, 27, 1229-1244.

[†] These authors contributed equally to this work.

**3. The Impact of Structural Modifications in Donor-Acceptor Systems on Homojunction Organic Solar Cell Photovoltaic Properties**

Daniel-Florin Bogoșel[1], **Gavril-Ionel Giurgi[1]**, Alexandru Balan, Alexandra Pop, Ion Grosu, Andreea Petronela Crișan, Anamaria Terec

*Organic Electronics*, 2025, 141, 107212.

[1] These authors contributed equally to this work.

**4. Structure-properties relationships in triarylamine-based push-pull systems-$C_{60}$ dyads as active material for single-material organic solar cells**

Alexandra Bogdan, Lorant Szolga, **Gavril-Ionel Giurgi**, Andreea Petronela Crișan, Diana Bogdan, Sarinya Hadsadee, Siriporn Jungsuttiwong, Riccardo Po, Ion Grosu, Jean Roncali

*Dyes and Pigments*, 2021, **184**, 108845.

**5. Exploring the Optoelectronic Properties of D-A and A-D-A 2,2'-bi[3,2-b]thienothiophene Derivatives**

Levi Gabrian, **Gavril-Ionel Giurgi**, Ioan Stroia, Elena Bogdan, Andreea Petronela Crișan, Niculina Daniela Hădade, Ion Grosu, Anamaria Terec

*Molecules*, 2022, 27, 8463.

**6. Mono- and di-substituted pyrene-based donor-π-acceptor systems with phenyl and thienyl π-conjugating bridges**

Monica Irina Nan, Eszter Lakatos, **Gavril Ionel-Giurgi**, Lorant Szolga, Riccardo Po, Anamaria Terec, Siriporn Jungsuttiwong, Ion Grosu, Jean Roncali

*Dyes and Pigments*, 2020, 181, 108527.

**7. Inverted versus direct structure bulk heterojunction organic solar cells involving a triphenylamine-based small molecular donor**

**Gavril-Ionel Giurgi**, Lorant Szolga, Istvan Kovacs, Elena Bogdan, Niculina Daniela Hădade, Anamaria

Terec, Ion Grosu, Jean Roncali
*Studia Universitatis Babeș-Bolyai Chemia*, 2020, 65, 95-106.

**8. Photovoltaic performances of two triarylamine-based donors in various inverted cell configurations**
**Gavril-Ionel Giurgi**, Lorant Szolga, Andreea Crișan, Ion Grosu, Jean Roncali
*Studia Universitatis Babeș-Bolyai Chemia*, 2021, 66, 97-105.

**9. Bulk and bilayer inverted organic solar cells (OSCs) exhibiting D-A and A-D-A donors with 2,2'-bi[3,2-b]thienothiophene units and $PC_{61}BM$ or $C_{70}$ acceptors**
Levi Gabrian, **Gavril-Ionel Giurgi**, Lorant Szolga, Andreea Petronela Crișan, Elena Bogdan, Ramona Gălătuș, Anamaria Terec, Ion Grosu
*Studia Universitatis Babeș-Bolyai Chemia*, 2023, 68, 275-283.

**10. Procedeu pentru obținerea de celule solare organice stabile de tipul ITO/ZnO/donor + acceptor/ $MoO_3$/Al folosind un donor de tip indacenoditiofenic și acceptori fulerenici ($PC_{61}BM$)** Terenti Natalia, **Giurgi Gavril-Ionel**, Szolga Lorant Andras, Grosu Ion
Brevet de invenție, RO 134664 B1, 2023.

**11. Procedeu pentru obținerea prin depunerea în vid înaintat de celule solare organice stabile de tipul ITO/ZnO/acceptor/donor/$MoO_3$/Al (celule "bilayer" inverse) folosind un donor de tip metildifenilamină și un acceptor fulerenic ($C_{70}$)**
**Giurgi Gavril-Ionel,** Szolga Lorant, Bogdan Alexandra, Crișan Andreea Petronela, Grosu Ion
Brevet de invenție depus la OSIM, Nr. înregistrare: A/00469, Data: 01.08.2022.